Machine Copy for Proofreading, Vol. x, y–z, 2013

THREE DIMENSIONAL RADAR COINCIDENCE IMAGING

Dongze Li*, Xiang Li, Yongqiang Cheng, Yuliang Qin, and Hongqiang Wang

Institute of Space Electronic Technology, School of Electronic Science and Engineering, National University of Defense Technology, Changsha, China

Abstract—Two dimensional (2D) radar coincidence imaging is an instantaneous imaging technique which can obtain 2D focused high-resolution images using a single pulse without the limitation to the target relative motions. This paper extends the imaging method to three dimensions. Such a three-dimensional (3D) radar imaging technique does not rely on Doppler frequency for resolution and has an extremely short imaging time (shorter than a pulse width), resulting in two remarkable properties: 1) it does not require the relative rotation between targets and radar; 2) it can considerably avoid the image blurring in processing noncooperative targets without motion compensation. 3D radar coincidence imaging consequently can derive high-quality images for either the targets that are stationary with respect to radars or the ones in maneuvering 3D rotations. The validity of the proposed imaging technique is confirmed by numerical simulations.

1. INTRODUCTION

Various radar imaging techniques are developed to extract 3D target shape information. The interferometric synthetic aperture radar imaging employs multiple antennas with different heights, where the third dimension of the target image is obtained via the phase difference of different ISAR images [1]. The snapshot imaging technique in [2] derives target 3D images via the processing of fusing multiple 2D ISAR images in different view angles. The 3D imaging algorithms in [3] are proposed for the near field turning table targets with the knowledge of

Received 11 August 2013.

* Corresponding author: Dongze Li (dongzeli1010@126.com).

the target motions through the measurements. Despite the different forms 3D radar imaging takes, most of the methods are based on the range-Doppler (RD) principle, where target information is derived via the processing of measuring range and changes in range [4]. This imaging principle requires the relative rotation between targets and radars to produce high azimuth resolution unless the radar system has a considerably large-scale antenna array to accomplish large aspect-angle variation [5]. Therefore, the synthetic aperture radar imaging technique is widely employed which is effective to derive high azimuth resolution via target relative rotation during the coherent integration time (CIT). Then another well-known requirement comes out that the target relative motion should be uniform during the CIT [5]. Obviously, it affects the applicability of imaging the noncooperative targets in complex maneuvers. The noncooperative motion yields time-varying Doppler frequency which destroys the Fourier-based imaging formation and would badly blur the images beyond recognition [6]. A long CIT (or a large aspect-angle integration) indeed provides the desired resolution, but meanwhile the nonuniform space sampling will produce smeared images which are difficult to be refocused even though various motion compensation algorithms are applied [6–8].

In consideration of aforementioned reasons, our recent work in [9] developed an instantaneous 2D imaging technique: radar coincidence imaging, which was motivated by classical coincidence imaging in optical systems [10]. Such an imaging method can obtain high-resolution well-focused images using just a single pulse without the limitation to target relative motion. Radar coincidence imaging resolves target scattering centers via the processing of measuring the independent waveforms of their echoes, which is quite different from conventional radar imaging methods based on the RD principle. Therefore, the method does not rely on Doppler frequency for resolution and has a considerably short imaging time. Consequently, radar coincidence imaging can achieve high imagery quality either for stationary targets or for maneuvering ones. Then the extension of this imaging method to three dimensions will potentially present the advantages as well. However, 3D scenario makes distinct differences in both the signal model and the conditions to perform such an imaging technique. Therefore, this paper develops 3D radar coincidence imaging which can provide target 3D images using a single pulse without the requirement for the knowledge of target motion parameters. Furthermore, the proposed 3D imaging method can achieve high-quality images for both the targets that are stationary with respect to radars and the ones in 3D maneuvering rotations.

The remaining sections are organized as follows. Section 2

analyzes the basic principles of the proposed imaging method. Section 3 shows the examples of 3D radar coincidence imaging. Section 4 concludes the work.

2. BASIC PRINCIPLES

The essence of radar coincidence imaging is to produce the signals presenting time-space independence in the detecting area. That is, the detecting signals in different positions or at different time instants are independent with each other. Such detecting signals will make target scattering centers within a beam reflect echoes of independent waveforms. Then the coincidence processing will extract the target scattering spatial distribution from the receiving signal.

As shown in Fig. 1, 3D radar coincidence imaging employs an array of N transmitters and a receiver. Generally, target location can be firstly estimated by current detection and localization techniques [11–13], which is defined as the center of the imaging region. Then an XYZ coordinate is built at the center of the imaging region labeled as I. The position vectors of the n-th transmitter and the receiver are $\mathbf{R}_n$ and $\mathbf{R}_r$, respectively (the imaging process is discussed within a radar pulse and then based on the stop-and-shoot model targets are assumed to be stationary during the very short observation interval [11]). $St_n(t)$ is the transmitting signal of the n-th transmitter. Here the imaging region I is required to be discretized to L imaging cells and every imaging cell is approximately regarded as its own centre, expressed as $I = \{\mathbf{r}_l\}_{l=1}^{L}$, $\mathbf{r}_l$ being the position vector of the l-th imaging cell center. Then the detecting signals distributed in the imaging region is denoted as $S_I(\mathbf{r}, t)$, where $\mathbf{r}$ is the position vector of an arbitrary

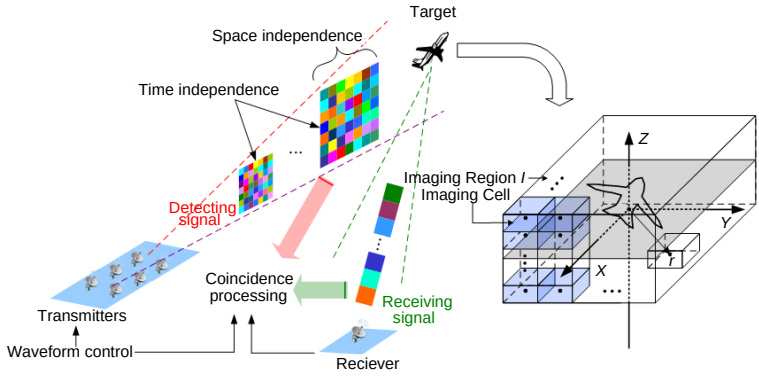

Figure 1. Geometry of 3D radar coincidence imaging.

imaging cell within I. To produce the time-space independent $S_I(\mathbf{r},t)$ via single transmitting, the transmitting signals are supposed to be group-orthogonal and time-independent [9], expressed as,

$$R_T(n_1,n_2;t_1,t_2)=\int St_{n_1}(t-t_1)St_{n_2}(t-t_2)dt=\delta(t_1-t_2)\cdot\delta(n_1-n_2) \quad (1)$$

where $St_n(t)=\mathrm{rect}(\frac{t}{T_p})\cdot st_n(t)$, $st_n(t)$ is the envelope function, T_p is the pulse width. Then the detecting signal $S_I(\mathbf{r},t)$ is,

$$S_I(\mathbf{r},t)=\sum_{n=1}^{N}St_n\left(t-\frac{|\mathbf{r}-\mathbf{R}_n|}{c}\right) \quad (2)$$

The self-correlation of $S_I(\mathbf{r},t)$ turns out to be,

$$\begin{aligned}R_I\left(\mathbf{r},\mathbf{r}';\tau,\tau'\right)&=\int S_I(\mathbf{r},t-\tau)S_I^*\left(\mathbf{r}',t-\tau'\right)dtdt\\&=\sum_{n=1}^{N}\sum_{n'=1}^{N}R_T\left(n,n';\frac{|\mathbf{r}-\mathbf{R}_n|}{c}+\tau,\frac{|\mathbf{r}'-\mathbf{R}'_n|}{c}+\tau'\right)\\&=\sum_{n=1}^{N}\delta\left(|\mathbf{r}-\mathbf{R}_n|-|\mathbf{r}'-\mathbf{R}_n|-c\left(\tau'-\tau\right)\right) \quad (3)\end{aligned}$$

If the target range $|\mathbf{R}_n|$ is much larger than the target size we have the approximation $|\mathbf{r}-\mathbf{R}_n|=|\mathbf{R}_n|-\mathbf{r}\cdot\mathbf{D}_n$ [4], where $\mathbf{D}_n$ is the unit direction vector of $\mathbf{R}_n$ and is expressed as $\mathbf{D}_n=(\cos\theta_n\cos\varphi_n,\cos\theta_n\sin\varphi_n,\sin\theta_n)^T$, herein θ_n and φ_n being the pitch angle and the azimuth angle. Then, (3) becomes,

$$R_I\left(\mathbf{r},\mathbf{r}';\tau,\tau'\right)=\sum_{n=1}^{N}\delta\left(\mathbf{D}_n^T\Delta\mathbf{r}-c\Delta\tau\right) \quad (4)$$

where $\Delta\tau=\tau'-\tau$, and $\Delta\mathbf{r}=\mathbf{r}'-\mathbf{r}=(\Delta x,\Delta y,\Delta z)^T$. Obviously, the value of $R_I(\mathbf{r},\mathbf{r}';\tau,\tau')$ is determined by the relationship between $c\Delta\tau$ and $\{\mathbf{D}_n^T\Delta\mathbf{r}\}_{n=1}^N$. In 2D case, $R_I(\mathbf{r},\mathbf{r}';\tau,\tau')$ can reach its maximum only when $\Delta r=0$, $\Delta\tau=0$ if there exist more than two transmitters [9]. In 3D case, we analyze the possible results through the following equation.

$$\begin{pmatrix}\cos\theta_1\cos\varphi_1 & \cos\theta_1\sin\varphi_1 & \sin\theta_1\\ \cos\theta_2\cos\varphi_2 & \cos\theta_2\sin\varphi_2 & \sin\theta_2\\ \vdots & \vdots & \vdots\\ \cos\theta_N\cos\varphi_N & \cos\theta_N\sin\varphi_N & \sin\theta_N\end{pmatrix}\cdot\begin{pmatrix}\Delta x\\ \Delta y\\ \Delta z\end{pmatrix}=\begin{pmatrix}c\Delta\tau\\ c\Delta\tau\\ \vdots\\ c\Delta\tau\end{pmatrix} \quad (5)$$

where we denote the coefficient matrix of (5) with D. Note that the transmitters we employed for 3D radar coincidence imaging are more than 3, i.e., $N > 3$, and the N transmitters are noncollinear leading to the noncoplanar $\{\mathbf{D}_n\}$. Thus $\text{rank}(D) = 3$. Without loss of generality, we choose the first four rows to calculate the fourth-order determinant of the corresponding augmented matrix of (5), labeled as $\tilde{D}$. Then we have

$$\det\left(\tilde{D}\right) = c\Delta\tau \cdot [(\mathbf{D}_1 - \mathbf{D}_2) \times \mathbf{D}_3 \cdot \mathbf{D}_4 + (\mathbf{D}_3 - \mathbf{D}_4) \times \mathbf{D}_1 \cdot \mathbf{D}_2] \quad (6)$$

where "$\times$" and "$\cdot$" denote the outer product and the inner product, respectively. For simplicity, we use the denotation of $\Theta = [(\mathbf{D}_1 - \mathbf{D}_2) \times \mathbf{D}_3 \cdot \mathbf{D}_4 + (\mathbf{D}_3 - \mathbf{D}_4) \times \mathbf{D}_1 \cdot \mathbf{D}_2]$. When $\Theta = 0$, $\text{rank}(\tilde{D}) = \text{rank}(D) = 3$. Then the Equation (5) has a nonzero solution when $\Delta\tau \neq 0$. It indicates that $R_I(\mathbf{r}, \mathbf{r}'; \tau, \tau')$ can reach its maximum, namely N, when $\Delta r \neq 0$, $\Delta\tau \neq 0$.

Let us focus on the case of $\Theta \neq 0$.

- When $\Delta\tau = 0$, $\det(\tilde{D}) = 0$, leading to $\text{rank}(\tilde{D}) = \text{rank}(D) = 3$. Thus, the equation has the unique solution of 0, which indicates $R_I(\mathbf{r}, \mathbf{r}'; \tau, \tau')$ can reach its maximum of N only under the condition of $\Delta\mathbf{r} = 0$, $\Delta\tau = 0$.
- When $\Delta\tau \neq 0$, $\det(\tilde{D}) \neq 0$, leading to $\text{rank}(\tilde{D}) = 4 \neq \text{rank}(D)$. Thus, the equation has no solution, which indicates no $\Delta\mathbf{r}$ can make $R_I(\mathbf{r}, \mathbf{r}'; \tau, \tau')$ reach its maximum of N when $\Delta\tau \neq 0$.

Therefore, on condition that $\Theta \neq 0$, $R_I(\mathbf{r}, \mathbf{r}'; \tau, \tau')$ can reach its maximum only when $\Delta\mathbf{r} = 0$, $\Delta\tau = 0$. Actually, this condition is tractable to be achieved. For example, we consider 4 antennas where three of them are set to have the same pitch angle for simplicity, i.e., $\theta_1 = \theta_2 = \theta_3$. Then, we have, $\Theta = 4\cos^2\theta_1(\sin\theta_1 - \sin\theta_4)\sin\frac{\varphi_2-\varphi_1}{2} \cdot \sin\frac{\varphi_3-\varphi_2}{2} \cdot \sin\frac{\varphi_3-\varphi_1}{2}$. Because the direction vectors are different from each other, then $\varphi_1 \neq \varphi_2 \neq \varphi_3$, leading to $\sin\frac{\varphi_2-\varphi_1}{2} \cdot \sin\frac{\varphi_3-\varphi_2}{2} \cdot \sin\frac{\varphi_3-\varphi_1}{2} \neq 0$. Thus, $\Theta \neq 0$ will be guaranteed when $\theta_1 \neq (\theta_4 \text{ or } \pi - \theta_4) \neq \pm\pi/2$.

Based on the analysis above, we define the property as follows.

Property 1:

$$(\mathbf{D}_k - D_l) \times \mathbf{D}_m \cdot \mathbf{D}_n + (\mathbf{D}_m - \mathbf{D}_n) \times \mathbf{D}_k \cdot \mathbf{D}_l \neq 0, \quad m \neq n \neq k \neq l$$

When property 1 holds $R_I(\mathbf{r}, \mathbf{r}'; \tau, \tau')$ can reach the maximum of N only on condition that $\Delta\mathbf{r} = 0$, $\Delta\tau = 0$. Especially, if the antenna number is big, for example $N = 10$, the result of (4) could be viewed as an approximate delta function,

$$R_I\left(\mathbf{r}, \mathbf{r}'; \tau, \tau'\right) \sim N\delta\left(\mathbf{r} - \mathbf{r}', \tau' - \tau\right) \quad (7)$$

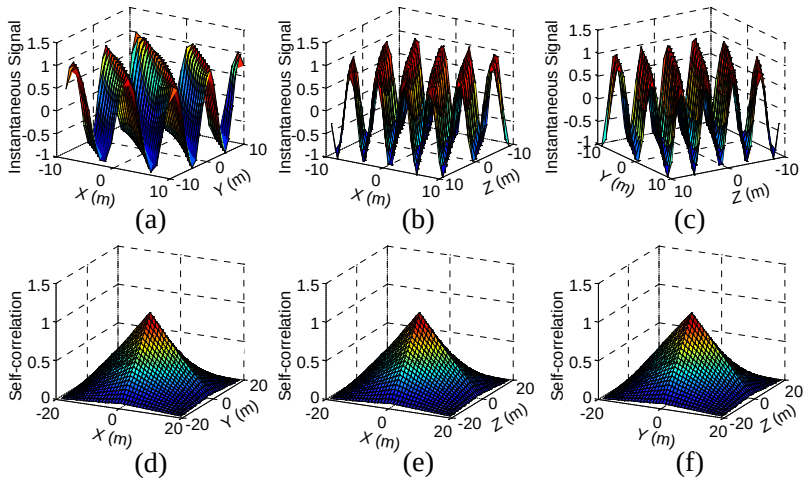

Figure 2. The spatial distribution of the LFM signals. (a) The spatial distribution in XY plane. (b) The spatial distribution in XZ plane. (c) The spatial distribution in YZ plane. (d) The spatial self-correlation in XY plane. (e) The spatial self-correlation in XZ plane. (f) The spatial self-correlation in YZ plane.

Thus (7) indicates that the detecting signal with the characteristic of approximate time-space independence can be generated in three dimensions, which is the essence to perform 3D radar coincidence imaging. To look into the spatial distribution of such detecting signals, we illustrate the $S_I(t, \mathbf{r})$ at an arbitrary instant in an imaging region I which is 10 km away from the radar system. Herein the group-orthogonal and time-independent transmitting signals are generated via imposing the zero-mean Gaussian-noise modulation on amplitude, expressed as,

$$St_n(t) = A_n(t) \exp\left[j\left(2\pi f t + \phi\right)\right] \cdot \mathrm{rect}\left(\frac{t}{T_p}\right) \tag{8}$$

where f is the carrying frequency, and ϕ is the initial phase. $\{A_n(t)\}_{n=1}^{N}$ is the mutual-independent Gaussian-noise, where $R_A(n_1, n_2; t_1, t_2) = \delta(n_1 - n_2, t_1 - t_2)$. Then, $R_T(n_1, n_2; t_1, t_2) = \exp[j2\pi f(t_2 - t_1)] \cdot R_A(n_1, n_2; t_1, t_2) = \delta(n_1 - n_2, t_1 - t_2)$. Additionally, for the sake of comparison, we also depict the detecting signals produced by the linear frequency modulated (LFM) signal which is an instance of the coherent signals. Fig. 2 and Fig. 3 illustrate the instantaneous spatial distribution of the detecting signals in the XY, XZ, and YZ plane, and their respective self-correlation is also given.

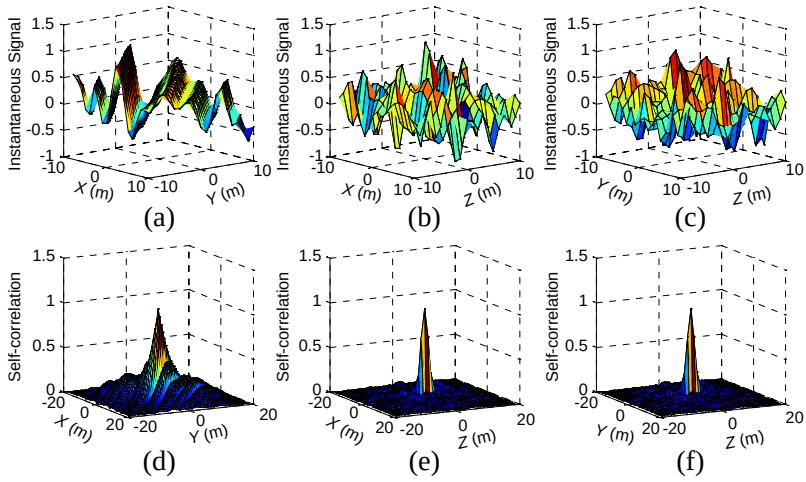

Figure 3. The spatial distribution of the time-independent signals. (a) The spatial distribution in XY plane. (b) The spatial distribution in XZ plane. (c) The spatial distribution in YZ plane. (d) The spatial self-correlation in XY plane. (e) The spatial self-correlation in XZ plane. (f) The spatial self-correlation in YZ plane.

Clearly, signal distribution generated by the LFM waveforms exhibits marked spatial correlation. By contrast, time-independent waveforms can produce the detecting signals that fluctuate incoherently versus positions.

Then, we express the receiving signal as the superposition of $S_I(\mathbf{r}, t)$,

$$Sr(t) = \sum_{l=1}^{L} \sigma_l S_I \left(\mathbf{r}_l, t - \frac{|\mathbf{r}_l - \mathbf{R}_r|}{c} \right) \tag{9}$$

where σ_l is the scattering coefficient of the l-th imaging cell, and for the imaging cell without target scattering center $\sigma_l = 0$. Particularly, the coincidence imaging formulism needs a reference signal [14], which can be structured as,

$$S(\mathbf{r}, t) = S_I \left(\mathbf{r}, t - \frac{|\mathbf{r} - \mathbf{R}_r|}{c} \right) \tag{10}$$

Obviously, the reference signal $S(\mathbf{r}, t)$ is just the transform of $S_I(\mathbf{r}, t)$ with an additional time-delay induced by the propagation to the

receiver. Then, (9) becomes,

$$Sr(t) = \sum_{l=1}^{L} \sigma_l S\left(\mathbf{r}_l, t\right) \tag{11}$$

Therefore, the scattering coefficient σ_x of an arbitrary imaging cell $\mathbf{r}_x$ can be explicitly obtained via the correlation between the receiving signal and $S(\mathbf{r}_x, t)$,

$$\begin{aligned} \int Sr\left(t\right) S^*\left(\mathbf{r}_x, t\right) dt &= \sum_{l=1}^{L} \sigma_l \cdot R_I\left(\mathbf{r}_l, \mathbf{r}_x; \frac{|\mathbf{r}_l - \mathbf{R}_r|}{c}, \frac{|\mathbf{r}_x - \mathbf{R}_r|}{c}\right) \\ &\sim \sum_{l=1}^{L} \sigma_l \cdot N\delta\left(\mathbf{r}_l - \mathbf{r}_x\right) = N \cdot \sigma_x \end{aligned} \tag{12}$$

That is,

$$\sigma_x \sim \frac{1}{N} \int Sr\left(t\right) S^*\left(\mathbf{r}_x, t\right) dt \tag{13}$$

Since the detecting signal $S_I(\mathbf{r}, t)$ or $S(\mathbf{r}, t)$ can be computed according to the known transmitting waveforms, the scattering coefficient of every imaging cell will be extracted from the receiving signal as denoted in (13). Obviously, the higher time-space independent degree the detecting signals present, the better resolution this correlation can provide. Thus, the 3D target image can be obtained as long as the transmitting signals can generate the time-space independent detecting signals by satisfying the condition in (1).

The essence of 3D radar coincidence imaging consists in that the superposition of multiple transmitting signals with the characteristic of time-independence and group-orthogonality increases the variety of detecting-signal spatial distribution, so that the scattering centers within a beam reflect echoes of different waveforms associated with their respective locations. As well known, the 3D imaging techniques based on the RD principle generally employs coherent signals and resolves target scattering centers by extracting the differences of time-delay and Doppler gradient in their echoes. However, for the proposed imaging method, scattering center echoes do not just differ from each other upon time-delay or Doppler frequency, and above all their waveforms are highly different which provides alternative information for distinguishing themselves. Especially, this resolvable feature does not need aspect-angle integration or large-scale antenna array, which could be achieved using only a single returned pulse. Due to the very short imaging time, the influence of the target noncooperative motion on imagery qualities will be considerably reduced. In addition,

3D radar coincidence imaging does not require target rotation for resolution. Therefore, high-quality images could be derived for either noncooperative targets or stationary ones.

Note that the perfect point-to-point relationship as denoted in (13) depends on the highly time-space independent detecting signals, which is mainly achieved by the time-independent transmitting signals. However, the complete time-independence denoted as (1) is almost impossible for either simulation data or actual radar signal. Thus, the incompletely time-independent transmitting signal would degrade the spatial independence of the detecting signal. As shown in Fig. 3, despite the spatial incoherence the signals on adjacent positions remain correlated to a certain extent and it is far from the desired spatial independence as required in (7). It has been demonstrated in [9] that the time-independent degree of microwave transmitting signals is inadequate to extract the target scattering coefficient with high resolution. Consequently, only the correlation between $Sr(t)$ and $S(\mathbf{r}, t)$ cannot generate a high resolution for radar coincidence imaging.

Therefore, a parameterized approach is employed to rebuild target images, which is less restricted by the independence of detecting signals. The approach utilizes the relationship between the receiving signal and the reference signal as denoted in (11) to structure a radar coincidence imaging equation, given as follows.

$$\mathbf{Sr} = \mathbf{S} \cdot \boldsymbol{\sigma}$$

$$\begin{bmatrix} S\mathbf{r}(t_1) \\ S\mathbf{r}(t_2) \\ \vdots \\ S\mathbf{r}(t_K) \end{bmatrix} = \begin{bmatrix} S(\mathbf{r}_1, t_1) & S(\mathbf{r}_2, t_1) & \dots & S(\mathbf{r}_L, t_1) \\ S(\mathbf{r}_1, t_2) & S(\mathbf{r}_2, t_2) & \dots & S(\mathbf{r}_L, t_2) \\ \vdots & \vdots & \dots & \vdots \\ S(\mathbf{r}_1, t_K) & S(\mathbf{r}_2, t_K) & \dots & S(\mathbf{r}_L, t_K) \end{bmatrix} \cdot \begin{bmatrix} \sigma_1 \\ \sigma_2 \\ \vdots \\ \sigma_L \end{bmatrix} \tag{14}$$

where $\mathbf{S}$ is the reference signal matrix, $\mathbf{Sr}$ is the vector of the receiving signal, and $\boldsymbol{\sigma}$ is the unknown vector of the scattering coefficient. The coincidence imaging equation will have a unique solution on condition that $\mathbf{S}$ is nonsingular. Hence, the time samples firstly should not be less than the imaging cells. Then the columns and the rows of $\mathbf{S}$ basically represent the detecting signals in different positions and at different instants. Thus, the row rank and the column rank of $\mathbf{S}$ are determined by the independence of the detecting signal in time and space, respectively. Therefore, the time-space independence characteristic denoted in (7) would ensure a full-rank $\mathbf{S}_{L\times L}$, based on which $\boldsymbol{\sigma}$ can be uniquely recovered.

After the analysis above, we now summarize the imaging scheme as follows.

Step 1. Estimate the location of the target center and define it as the center of the imaging region.

Step 2. Discretize the imaging region to form $I = \{\mathbf{r}_l\}_{l=1}^{L}$.

Step 3. Compute the reference signal $\{S(\mathbf{r}_l, t)\}_{l=1}^{L}$.

Step 4. Draw out L samples from $\{S(\mathbf{r}_l, t)\}_{l=1}^{L}$ in time domain to form $\mathbf{S}_{L\times L}$.

Step 5. Draw out L samples from $\mathbf{Sr}(t)$ at the same sample points to form $\mathbf{Sr}$.

Step 6. Solve the equation $\mathbf{Sr} = \mathbf{S} \cdot \boldsymbol{\sigma}$.

Obviously, the image-reconstruction or the achievement of resolution depends on whether the coincidence imaging equation can be solved. Therefore, an explicit resolution is determined by quantitative solvable conditions. However, as well known, there have not been applicable criterions to evaluate such conditions or the resolution of the parameterized method in existing approaches. Thus, as a special subject, this unsolved problem is a focus in our current work.

3. RESULTS USING PHANTOMS

In this section, several examples are designed to demonstrate the imaging results of the proposed method. Herein we use an N-transmitter 1-receiver array, which consists of 6 antennas, as shown in Fig. 4. The positions of the radar array and the imaging region satisfy property 1. The transmitting signals used for simulation are denoted in (8). In consideration of noise impact in practical experiments, the imaging equation is rewritten as $\mathbf{Sr} = \mathbf{S} \cdot \boldsymbol{\sigma} + \mathbf{n}$, where $\mathbf{n}$ is modeled as white noise. The signal-noise-ratio (SNR) is 20 dB. Other detailed parameters are given in Table 1.

For experiments of RD imaging techniques, the resolution can be clearly given according to bandwidth and beam width or coherent

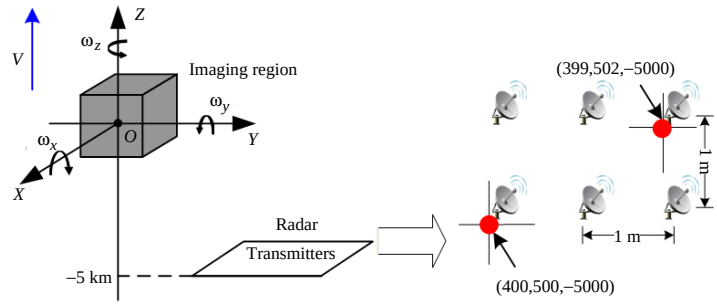

Figure 4. The geometry of imaging region and the antenna array.

Table 1. System parameters of the phantom experiments.

Description	Parameter	Value
Average transmitted power	P_t	10 W
Antenna gain	K	20 dB
Receiver sensitivity	$S_{\min}$	−90 dBm
Pulse repetition frequency	PRF	600 Hz
Carrier frequency	f_c	9.5 GHz
Pulse width	T_p	50 μs
Bandwidth	B	1 GHz
Sampling frequency	f_s	2 GHz

integration angle. As explained in the last section, however, a theoretical resolution of radar coincidence imaging is difficult to be provided. Nevertheless we try to analyze the resolution in this specific experiment scenario through numeric results. Note that radar antennas and imaging region are definite in the experiment. In this case, the detecting signals in the imaging region thus have been fixed. Then while the imaging cell gets smaller the independence of the signals from adjacent imaging cells is decreased and the incoherency of **S** becomes worse. Finally **S** will turn to be singular when the imaging-cell size decreases to a certain critical value. Therefore, this critical size of the imaging cell can be viewed as the resolution in this specific phantom. Fig. 5 depicts rank of **S** versus the imaging-cell size. To keep the real scale of target images, the imaging cell is set to have the equivalent height, length and width, denoted as l_c.

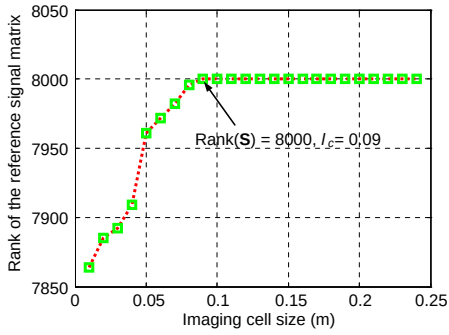

Figure 5. Rank of the reference signal matrix versus the imaging cell size.

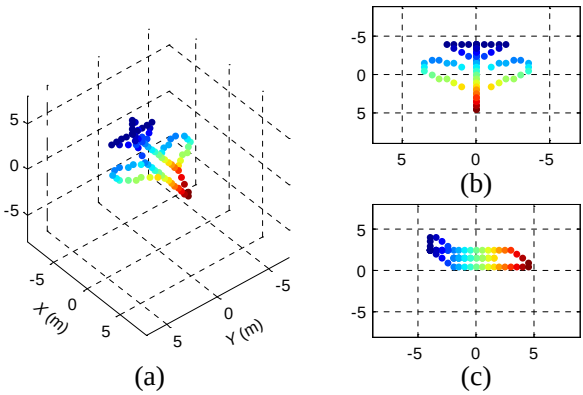

Figure 6. The target model. (a) The 3D view. (b) The vertical view. (c) The side view.

Based on the results of Fig. 5, a nonsingular $\mathbf{S}$ can be ensured if $l_c \geq 0.09\,\mathrm{m}$ in the experiment. Then the target model is shown in Fig. 6. As depicted in Fig. 4, the target has translational motion along with Z-axis, labeled as v, and also has 3D rotations along with the X-axis, Y-axis and Z-axis, which are denoted as ω_x, ω_y and ω_z, respectively. The target will be imaged in four scenes. They are, scene1: the target is stationary in noise-free environment; scene2: the target is stationary and SNR is 20 dB; scene3: the target motion is uniform and SNR is 20 dB, where $v = 300t$, and $\omega_x = \omega_y = \omega_z = 10t$; scene4: the target motion is nonuniform and SNR is 20 dB, where $v = 300t + 50t^2$, and $\omega_x = 10t + 10t^2 + 20t^3 + 20t^4$, $\omega_y = 11t + 15t^2 + 25t^3 + 25t^4$, $\omega_z = 8t + 10t^2 + 35t^3 + 25t^4$. Here the rotations are all referred in angle measurement.

As mentioned in the imaging scheme, target initial position and its first-order translational velocity are estimated firstly to obtain the target location, where the estimation precision is 70%. Then the imaging region is set to $10\,\mathrm{m} \times 10\,\mathrm{m} \times 10\,\mathrm{m} = 1000\,\mathrm{m}^3$, and is discretized to $20 \times 20 \times 20 = 8000$ imaging cells with $l_c = 0.5\,\mathrm{m}$. A single pulse provides $T_P \times f_s = 100000$ time samples, from which we can choose 8000 samples to form the square matrix $\mathbf{S}$. Since $l_c = 0.5\,\mathrm{m} \geq 0.09\,\mathrm{m}$, $\mathbf{S}$ thus is nonsingular. Then the scattering-coefficient vector can be uniquely recovered as $\boldsymbol{\sigma} = \mathbf{S}^{-1}\mathbf{Sr}$, where the inverse matrix $\mathbf{S}^{-1}$ is estimated with the Matlab function "inv".

The imaging method implementation mainly consists of two parts, i.e., computing the detecting signals to obtain the reference signal matrix $\mathbf{S}$ and recovering the target image via computing $\boldsymbol{\sigma} = \mathbf{S}^{-1}\mathbf{Sr}$. On a single PC processor with 2.33 GHz CPU and 2 GB of memory,

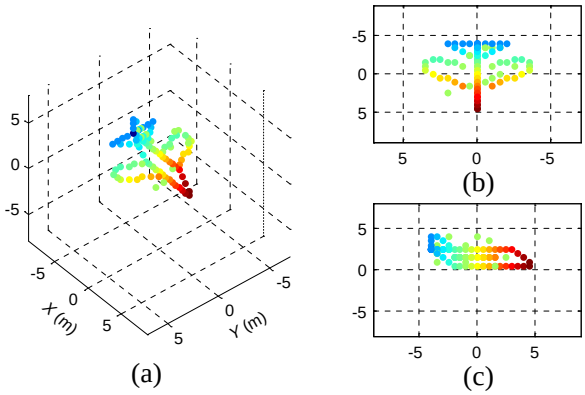

Figure 7. The noise-free imaging result of the stationary target. (a) The 3D view. (b) The vertical view. (c) The side view.

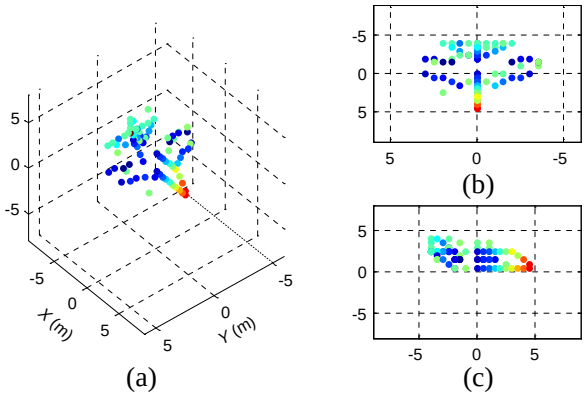

Figure 8. The imaging result of the stationary target when SNR = 20 dB. (a) The 3D view. (b) The vertical view. (c) The side view.

2 minutes are needed to compute the detecting signals, and 6 seconds are needed to recover the target image. The imaging results from scene1 to scene4 are shown in Fig. 7–Fig. 10.

As shown in Fig. 7, the estimation of the target scattering coefficients and positions are basically correct in noise-free environment. In the presence of white noise, the recognizable target image is also obtained, as shown in Fig. 8. By contrast, the noise-free recovery gives better estimation of the scattering coefficients. Then in Fig. 9 the target is well imaged when it is in uniform motions. It indicates that 3D radar coincidence imaging does not rely on the Doppler frequency gen-

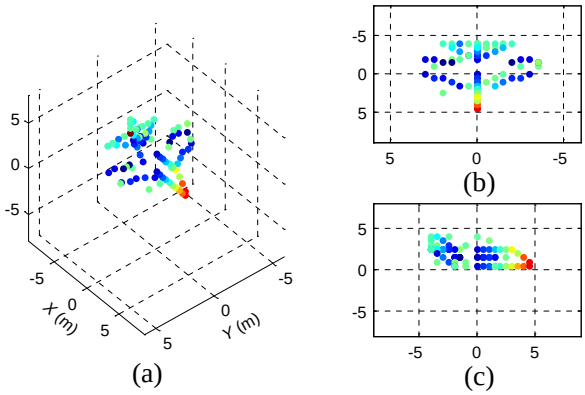

Figure 9. The imaging result of the uniformly moving target when SNR = 20 dB. (a) The 3D view. (b) The vertical view. (c) The side view.

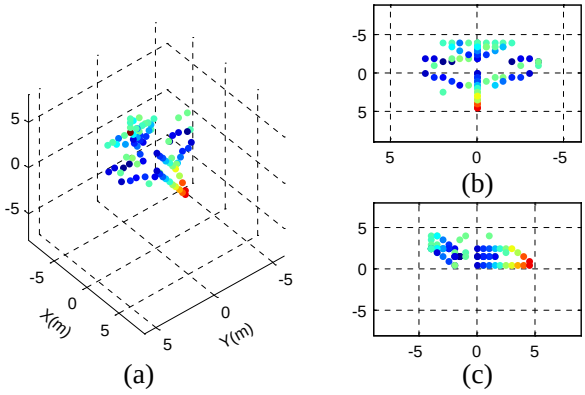

Figure 10. The imaging result of the maneuvering target when SNR = 20 dB. (a) The 3D view. (b) The vertical view. (c) The side view.

erated by target relative rotation. Especially, the fine imagery quality is maintained even when the target is involved in marked noncooperative rotation, as shown in Fig. 10. Herein, we use 8000 consecutive samples. Thus, the imaging time (the time of observing the target) is $8000/f_s = 4\,\mu$s. Due to this very short imaging time, the effect of the high-order motion components is highly decreased. Thus, the nonuniform rotation here does not blur the imaging result even though these high-order components are not compensated. Therefore, the imaging results above indicate that the 3D radar coincidence imaging method

can derive high-quality 3D reconstruction for both stationary targets and maneuvering ones.

4. CONCLUSION

This paper proposes the 3D radar coincidence imaging method which can provide target 3D images using a single pulse without the requirement for motion parameter knowledge. This method can derive high-quality images either for the targets which are stationary with respect to radars or for the ones in 3D maneuvering rotations. The validity and the applicability of the proposed method are demonstrated in simulations. For the future study, to provide a theoretical resolution of 3D radar coincidence imaging might be of the most interest. In addition, the imaging performance under different SNR conditions, the antenna array design as well as the computation complexity are worth of further considerations.

REFERENCES

1. Soumekh, M., "Automatic aircraft landing using interferometric inverse synthetic aperture radar imaging," *IEEE Trans. Image Process.*, Vol. 5, No. 9, 1335–1345, Sep. 1996.
2. Mayhan, J. T., et al., "High resolution 3D snapshot ISAR imaging and feature extraction," *IEEE Trans. Aerosp. Electron. Syst.*, Vol. 37, No. 2, 630–642, 2001.
3. Fortuny, J., "An efficient 3-D near-field ISAR algorithm," *IEEE Trans. Aerosp. Electron. Syst.*, Vol. 34, No. 4, 1261–1270, 1998.
4. Ausherman, D. A., A. Kozma, J. L. Walker, H. M. Jones, and E. C. Poggio, "Developments in radar imaging," *IEEE Trans. Aerosp. Electron. Syst.*, Vol. 20, No. 4, 363–400, Jul. 1984.
5. Bao, Z., M. D. Xing, and T. Wang, *Radar Imaging Technique*, Publish House Electron. Ind., Beijing, 2005.
6. Chen, V. C. and H. Ling, *Time Frequency Transforms for Radar Imaging and Signal Analysis,* Artech House, MA, 2002.
7. Itoh, T., H. Sueda, and Y. Watanabe, "Motion compensation for ISAR via centroid tracking," *IEEE Trans. Aerosp. Electron. Syst.*, Vol. 32, No. 3, 1191–1197, 1996.
8. Thayaparan, T., G. Lampropoulos, S. K. Wong, and E. Riseborough, "Application of adaptive joint time-frequency algorithm for focusing distorted ISAR images from simulated and measured radar data," *IEE Proc. — Radar Sonar Navig.*, Vol. 150, No. 4, 213–220, Aug. 2003.

9. Li, D., et al., "Radar coincidence imaging: An instantaneous imaging technique with stochastic signals," *IEEE Trans. Geosci. Remote Sens.*, Vol. PP, No. 99, 1, 2013, Online Available: http://dx.doi.org/10.1109/TGRS.2013.2258929.
10. Shih, Y., "Quantum imaging," *IEEE Journal of Selected Topics in Quantum Eletronics,* Vol. 13, No. 4, 1016–1030, Jul./Aug. 2007.
11. Margaret, C. and B. Brett, *Fundamentals of Radar Imaging,* SIAM, PA, 2009.
12. Liu, H.-Q., H.-C. So, K. W. K. Lui, and F. K. W. Chan, "Sensor selection for target tracking in sensor networks," *Progress In Electromagnetics Research*, Vol. 95, 267–282, 2009.
13. Liu, H.-Q. and H.-C. So, "Target tracking with line-of-sight identification in sensor networks under unknown measurement noises," *Progress In Electromagnetics Research*, Vol. 97, 373–389, 2009.
14. Gatti, A., E. Brambilla, M. Bache, and L. A. Lugiato, "Ghost imaging with thermal light: Comparing entanglement and classical correlation," *Phys. Rev. Lett.*, Vol. 93, No. 9, 093602(1)–093602(4), 2004.